

# Fast and Effective Robustness Certification for Recurrent Neural Networks

Wonryong Ryou\*, Jiayu Chen\*, Mislav Balunović\*, Gagandeep Singh\*, Andrei Dan†, Martin Vechev\*

\*Department of Computer Science, ETH Zürich  
Zürich, Switzerland

†ABB Corporate Research  
Baden, Switzerland

**Abstract**—We present a precise and scalable verifier for recurrent neural networks, called R2. The verifier is based on two key ideas: (i) a method to compute tight linear convex relaxations of a recurrent update function via sampling and optimization, and (ii) a technique to optimize convex combinations of multiple bounds for each neuron instead of a single bound as previously done. Using R2, we present the first study of certifying a non-trivial use case of recurrent neural networks, namely speech classification. This required us to also develop custom convex relaxations for the general operations that make up speech preprocessing. Our evaluation across a number of recurrent architectures in computer vision and speech domains shows that these networks are out of reach for existing methods as these are an order of magnitude slower than R2, while R2 successfully verified robustness in many cases.

## I. INTRODUCTION

Prior work has demonstrated the susceptibility of recurrent neural networks (RNNs) to adversarial perturbations of its inputs [1]. Naturally, this exposed serious security vulnerabilities in state-of-the-art speech recognition models based on RNNs [2], [3] and models for other domains sharing the same architectures, such as malware detection [4]. Though RNNs have been outperformed by transformers [5] on some benchmarks, they are still widely used in many problems which require modelling long-term dependencies for lengthy sequential signals [6], [7], [8], [9]. Thus, verifying robustness of recurrent architectures is an important challenge towards deployment of these models in practice.

While there has been considerable interest in certifying the robustness of feedforward image classifiers, less attention has been given to recurrent architectures. Current solutions do not scale beyond simple models and datasets which limits their practical applicability. Further, to the best of our knowledge, there has been no work on verifying the robustness of speech recognition models based on recurrent architectures. In this work, we take a step in this direction and present a precise and scalable approach for certifying the robustness of practical and challenging recurrent architectures that enables the certification of realistic speech recognition systems for the first time ever.

We illustrate the problem setting and overall flow in Fig. 1. Here, an LSTM based speech recognition model receives a signal encoding the utterance of "stop" by a human. The signal

is sliced into several frames to be processed throughout the model pipeline. Since the environment in which such models are usually employed contains noise, it is essential that the model classifies small variations to original signal caused by the noise as "stop". Recent work [2] has shown that it is possible that the model classifies one of the perturbed signals as "go". Employing such a non-robust model in automated traffic control systems can result in accidents. Our goal in this work is then to formally establish security guarantees on the classification robustness of such models against noise induced perturbations. Given a correctly classified speech signal from the test set and a noise model which defines a set of input signals of interest, our method can automatically prove that all signals in the set are classified correctly and therefore the model is safe to use for such inputs. We focus on LSTMs as they are the most widely used form of RNNs, but our methodology can be easily extended to other architectures such as GRUs.

Fig. 1 shows how our proposed R2: Robustness certifier for Recurrent neural networks proves the robustness of the model. Here, the labeled rectangles represent the operations in the network we are certifying. The "Preprocess" boxes capture domain-specific pre-processing operations (typically present when using RNNs, e.g., speech processing). In our method, we compute a symbolic formula capturing all input speech signals that can be introduced to the model under the given perturbation measure. At each timestep  $i$ , pre-processing receives a polyhedral shape  $s^{(i)}$ . Certification of LSTMs is then based on propagating these polyhedral shapes symbolically through both the preprocessing operations and the LSTM network itself, and results in a polyhedral shape in the output, denoted as  $z$ . If  $z$  contains only output vectors which classify to the "stop" class, robustness of the LSTM network is established, but Fig. 1 shows that  $z$  is overlaying on "go" region as well, which tells there might be a noise making the model malfunctioning to classify "stop" to label "go".

**Key challenge: polyhedral relaxations for LSTMs** The key challenge to effective certification of LSTMs is the design of precise and scalable polyhedral overapproximations of non-linear operations: given a polyhedral shape capturing the hidden state  $h^{(i-1)}$ , to produce the shape capturing the next

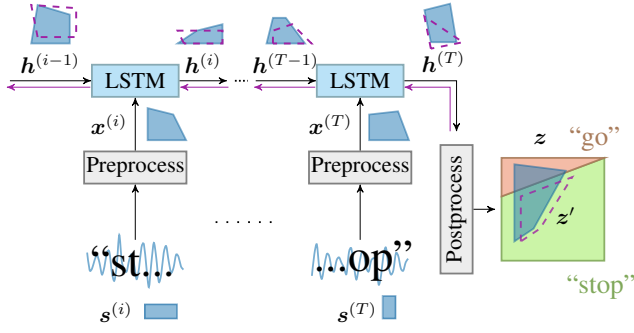


Fig. 1: End-to-end certification of RNNs with LSTM cells using R2: the utterance “stop” with some perturbation might not be classified to “stop” but “go”. We show how all possible perturbations are captured and propagated through the system, then refined backward for better precision.

state  $h^{(i)}$ . A recent method [10] computes this relaxation by using gradient-based optimization, but suffers from two major issues. First, the optimization procedure is expensive and does not scale to realistic use cases. Second, even if we disregard scalability, the method lacks convergence and optimality guarantees. To address these issues, we introduce a novel technique based on a combination of sampling and linear programming, which is significantly more precise and scalable than [10], while also offering asymptotic guarantees of convergence towards the optimal solution.

**Refinement via optimization** As mentioned earlier, to certify the property, we need to verify if each concrete point in the output shape  $z$  classifies to the correct label, “stop”. If this is true, then we have proved the output of the network is correct on all inputs in the input polyhedral regions  $s^{(1)}, \dots, s^{(T)}$ . However, as in Fig. 1, when we propagate these shapes through the network, due to over-approximation, it is possible to obtain an output shape  $z$  which contains spurious incorrect concrete points (it intersects the red region representing incorrect outputs). To address this issue, we form a loss based on the output shape, backpropagate the gradient of this loss through the timesteps and adjust the polyhedral relaxations in each LSTM unit to decrease the loss so that in the next try we arrive closer to certifying the network. This is demonstrated in Fig. 1 using the purple backward arrows with the new polyhedral shapes shown in purple. Finally, the new output shape  $z'$  (dashed purple) lies completely inside the green region of the output space, meaning it contains only provably correct output vectors (classifying to “stop”) and hence certification succeeds. As we show experimentally, this method significantly increases precision of end-to-end certification, without introducing large runtime costs. We remark that advances in certification introduced in our work are of interest beyond RNNs, especially the method to dynamically choose between different polyhedral relaxations.

**Key contributions** Our main contributions are:

- A novel and efficient method to certify robustness of recurrent neural networks to adversarial perturbations.

The method is based on new polyhedral relaxations which handle non-linear operations in LSTMs, are significantly more scalable and precise than prior work that allows verifying the larger models.

- A novel method which dynamically selects between multiple polyhedral relaxations in order to increase certification precision.
- An implementation of the method in a system called R2. We evaluated R2 on several benchmarks and datasets, showing it scales to realistic networks. Further, using R2, we were able to, for the first time, certify RNNs used in speech classification.

Based on our results, we believe that our work advances the state-of-the-art in formal reasoning of modern neural models.

## II. RELATED WORK

While the first adversarial examples for neural networks were found in computer vision [11], [12], recent work also showed the vulnerability of RNNs [1]. Modern speech recognition systems, based on RNNs, were shown susceptible to small noise crafted by an adversary using white-box attacks [13], [2], achieving 100% success rate against DeepSpeech [14]. These were later followed by inaudible attacks [15], universal perturbation [16], structural analysis [17], and adversarial music [3]. While providing a good empirical estimate of the vulnerability of RNNs, these works do not provide any robustness guarantees, which is the goal of our work.

Much recent work also aims at certifying neural networks, typically using SMT solving [18], abstract interpretation [19], [20], Lipschitz optimization [21], linear relaxations [22], [23], [24], [25], symbolic intervals [26], semi-definite relaxations [27] or combinations of methods [28], [29]. Another line of work considers using these relaxations to train provably robust neural networks [30], [31], [32], [33], [34], [35]. However, they do not train provably robust recurrent networks: to achieve this, our convex relaxations could be combined with these training methods.

There has also been recent work on certification of RNNs. [36] propose certification of RNNs based on mixed-integer linear programming, but it can only be applied to ReLU networks and does not work for LSTMs, which have sigmoid and tanh activations. [37] propose a discretization method to certify video models that are a combination of CNNs and RNNs. However, discretization does not scale to the perturbations we consider in our work. [38] address the certification of support vector machines for audio classification, but do not support neural networks. The most related work to ours is POPQORN [10], which proposes a method to certify RNNs. However, their approach is based on expensive gradient-based optimization for every single operation, which does not scale to practical applications such as audio classification, as we show in our experiments. [39], [40] propose to adjust the linear relaxations of activation functions, such as ReLU, tanh, and sigmoid by using projected gradient descent. Their approach shares the idea of learning the linear relaxation, but is restricted to feed-forward networks, and does not consider the more challenging

case of learning the convex combination of bounds for non-linearities in LSTMs. Recent work also certifies Transformers [41] using linear relaxations of non-linear operations in that architecture. However, they do not consider using multiple non-trivial linear relaxations as we do. [42] propose to verify RNNs by automatically inferring the temporal homogeneous invariants using binary search. However, their approach is limited to vanilla RNNs and does not apply to more commonly used LSTM networks which we consider in this work. [43] provide the randomized smoothing for speaker recognition, and [44] also consider the speech classification by the same approach with speech command dataset [45]. However, their target model is not recurrent and the perturbation metric is the volume change of the signal. Note that randomized smoothing is probabilistic as its name is, while we aim for deterministic certification.

### III. BACKGROUND

We first define a threat model that we work with and then present all operations that are part of the verification procedure, including speech preprocessing and LSTM updates.

#### A. Threat model

We define a threat model as an attacker is able to add at most  $\epsilon$  perturbation in  $L_\infty$  metric on the original input. The assumption is that the attacker can add any shift  $\delta$  to the original signal  $s$  so to obtain a perturbed signal  $s' = s + \delta$ . As  $L_\infty$  metric regulates the maximum perturbation along the all input sequence, no correlation between the perturbations on different positions exists. We treat the vector of intervals  $[s_i - \epsilon, s_i + \epsilon]$ , corresponding the element of original input  $s_i$ , as the input polyhedra to be certified through R2.

However, we need to mention the distinct threat model for speech classification following [2]. The measure of signal distortion are decibels (dB) defined as:

$$dB(s) = \max_i 20 \cdot \log_{10}(|s_i|); \quad dB_s(\delta) = dB(\delta) - dB(s)$$

Note that the quieter the perturbation is, the smaller  $dB_s(\delta)$  (it is usually a negative value as it is quieter than the signal) is. We fix the  $dB_s(\delta) =: \epsilon$  as  $dB$  perturbation and perform the verification over all perturbation  $\delta$  under this constraint.

Our goal of the robustness certification is to verify the model classifying  $s'$  as the same label of  $s$  under any  $\delta$  bounded by given  $\epsilon$ .

#### B. Long-Short Term Memory (LSTM)

LSTM architectures [46] are a key part of modern neural architectures as they can utilize long-term dependencies. These dependencies are passed through time using two state vectors

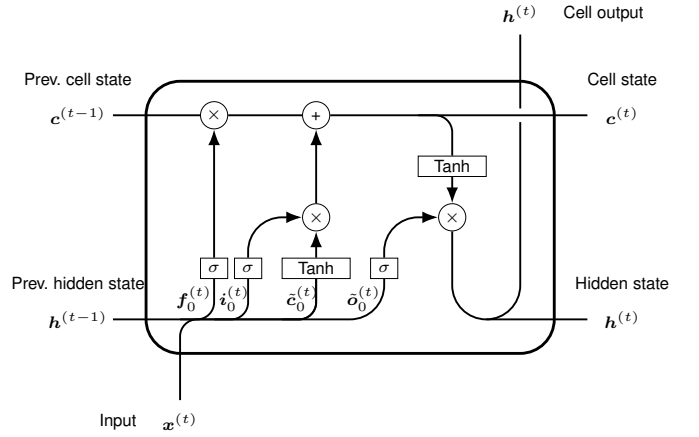


Fig. 2: LSTM cell illustration.  $f_0^{(t)}$ ,  $i_0^{(t)}$ ,  $o_0^{(t)}$ , and  $\tilde{c}_0^{(t)}$  represent the pre-activated gate. Each pre-activation's detail is described in Section III-B.

for the timestep  $t$ : cell state  $c^{(t)}$  and hidden state  $h^{(t)}$ . These state vectors are updated using the following formulas:

$$\begin{aligned} f_0^{(t)} &= [x^{(t)}, h^{(t-1)}]W_f + b_f \\ i_0^{(t)} &= [x^{(t)}, h^{(t-1)}]W_i + b_i \\ o_0^{(t)} &= [x^{(t)}, h^{(t-1)}]W_o + b_o \\ \tilde{c}_0^{(t)} &= [x^{(t)}, h^{(t-1)}]W_{\tilde{c}} + b_{\tilde{c}} \\ c^{(t)} &= \sigma(f_0^{(t)}) \odot c^{(t-1)} + \sigma(i_0^{(t)}) \odot \tanh(\tilde{c}_0^{(t)}) \\ h^{(t)} &= \sigma(o_0^{(t)}) \odot \tanh(c^{(t)}) \end{aligned}$$

where  $[\cdot, \cdot]$  is the horizontal concatenation two row vectors,  $W$  and  $b$  are kernel and bias of the cell, respectively. At timestep  $t$ , vectors  $f_0^{(t)}$ ,  $i_0^{(t)}$ ,  $o_0^{(t)}$ ,  $\tilde{c}_0^{(t)}$  represent pre-activations of the forget gate, input gate, output gate and the pre-calculation of a cell state, respectively. We show an illustration of an LSTM cell in Fig. 2. We treat  $\sigma$  and  $\tanh$  as forms of activation functions, which is why we define LSTM using pre-activations.

Intuitively, *input gate* transforms the input vector, *forget gate* filters the information from the previous cell state, *cell gate* transforms the current cell state, and *output gate* transforms the current hidden state. All of these gates receive as an input hidden state  $h^{(t-1)}$  of the previous cell and the input  $x^{(t)}$  to the current frame.

This recurrent architecture allows inputs with arbitrary length, allowing LSTM to handle temporal data, e.g. signal processing.

#### C. Speech preprocessing

Though there have been various works which operate directly on the raw signal [47], [48], the *filterbank method*, or *log Mel-filterbank energy*, is most widely used speech preprocessing. The final result of the transformation is a vector of coefficients whose elements contain log-scaled values of filtered spectra, one for every Mel-frequency. The idea of

filterbank is to model non-linear human acoustic perception as power spectrum filters based on Mel-frequencies. The overall steps are following:

- 1) *Pre-emphasizing and windowing*: Transform the signal with the pre-emphasizing and applying the Hamming window. This is to modify the signal into the difference between the adjacent sampled value and multiply them with sinusoidal Hamming function.
- 2) *Power spectrum of Fast Fourier transform (FFT)*: Perform the discrete Fourier transform (DFT) and obtain the squared norm of each element. FFT can be performed by matrix multiplication with complex entries, but we can modify it to use only real numbers by (i) separating real and imaginary parts of the matrix and constructing two separate matrices, (ii) multiplying each matrix with the signal, (iii) squaring the entries, and (iv) adding the resulting matrices entry-wise.
- 3) *Mel-filter bank log energy*: (i) We apply the Mel-filterbank to the power spectrum and (ii) take the log of the entries. As previously mentioned, applying filterbank is to filter the acoustically well-perceivable frequencies.

Following [49], each process can be represented by distinct matrix operation. It hence allows us to decompose and rearrange the steps into slightly different stages:

- 1) *Pre-square stage*:  $\mathbf{S} \rightarrow \mathbf{Y} = \mathbf{S}\mathbf{M}_1$  This stage contains pre-emphasizing, windowing (step 1), and FFT (until step 2-(ii) above). All the operations are representable using matrix multiplication, so we could calculate the matrix in advance.
- 2) *Square stage*:  $\mathbf{Y} \rightarrow \boldsymbol{\theta} = \mathbf{Y} \odot \mathbf{Y}$  This is step 2-(iii). Entry-wise square operation cannot be combined with other matrix multiplications.
- 3) *Pre-log stage*:  $\boldsymbol{\theta} \rightarrow \tilde{\mathbf{X}} = \boldsymbol{\theta}\mathbf{M}_2$  From step 2-(iv) through step 3-(i). Those are also combinable operations to single matrix.
- 4) *Log stage*:  $\tilde{\mathbf{X}} \rightarrow \mathbf{X} = \log \tilde{\mathbf{X}}$  Applying entry-wise logarithm, equivalent to step 3-(ii) above.

We use the resulting  $\mathbf{X} = [\mathbf{x}^{(1)} \dots \mathbf{x}^{(T)}]^{tr}$  as the input for the neural network.

#### IV. OVERVIEW

In this section, we first show the workings of our polyhedral LSTM certification on a small illustrative example. Next, we present a non-trivial combination of our proposed method with novel convex approximations for handling the non-linear operations applied in the speech preprocessing pipeline. The resulting combination yields for the first time precise and scalable formal guarantees on the robustness of challenging speech classifiers.

##### A. Single LSTM cell demonstration

Our goal is to certify robustness of a single LSTM cell with respect to the input  $x \in [-1.2, 1.2]$ . In this example, for the sake of simplicity, we assume there are two output classes and

all intermediate LSTM gates  $\{i, f, g, o\}$  share weight matrices and biases:

$$\begin{aligned} \{i, f, g, o\} &= \begin{bmatrix} 1 \\ 0.5 \end{bmatrix} x + \begin{bmatrix} 0 \\ 1 \end{bmatrix} \\ \mathbf{c} &= \sigma(\mathbf{i}) \odot \tanh(\mathbf{g}) \\ \mathbf{h} &= \sigma(\mathbf{o}) \odot \tanh(\mathbf{c}). \end{aligned}$$

To certify robustness, we need to prove that  $h_2 - h_1 > 0$  holds, implying the neural network classifies all inputs to the label 2.

1) *Interval bound propagation (IBP)*: We first show a common approach for certifying robustness based on IBP [26], [33], [32], [50], [51] which involves computing concrete lower and upper bounds for each neuron. While it is straightforward to apply IBP for verifying RNNs, it is usually quite imprecise in practice and therefore not suitable for our goal. This is because it disregards relationships between neurons that are created by propagating the input set through the various operations applied in LSTM. Applying IBP on our example, we obtain:

$$\begin{aligned} c_1 &\in [-0.64, 0.64] & h_1 &\in [-0.43, 0.43] \\ c_2 &\in [0.23, 0.77] & h_2 &\in [0.13, 0.54]. \end{aligned}$$

Using the above values results in an imprecise lower bound  $h_2 - h_1 \geq -0.30$  which incorrectly fails to prove robustness.

2) *Polyhedral relaxation via linear programming (LP)*: We address the precision limitations of IBP by computing relational polyhedral bounds for each neuron. To maintain scalability, we keep only one lower polyhedral and one upper polyhedral bound per neuron. To ensure optimality, we require having as 'small gap' as possible between the bounds. Such polyhedral relaxations are called *sound* when the area (volume) between the bounds contains all concrete values of the target function, i.e., it overapproximates the function.

##### Challenges in computing polyhedral bounds for LSTMs

Our abstraction for maintaining relational information is similar to [52], however the binary non-linear operations applied in LSTMs such as  $\sigma(x) \tanh(y)$  and  $\sigma(x)y$  are significantly more complex to handle than the ReLU, Sigmoid, and Tanh activations handled by [52]. This is because the non-linear operations in LSTMs mentioned above involve transcendental functions yielding non-linear 3D curves that are neither convex nor concave. The optimal polyhedral bounds for these operations have no closed-form solution and cannot be obtained by simple geometry or algebra. In fact, obtaining such bounds is computationally quite expensive [10]. For example, obtaining the lower linear plane for bounding  $\sigma(x) \tanh(y)$  is equivalent to solving a Lagrangian with 6 neurons - 3 linear coefficients, 2 interval-bounded coordinates and 1 Lagrange multiplier for the constraint. In contrast, the optimal polyhedral bounds for ReLU, Sigmoid, and Tanh have closed form solutions that can be easily visualized in 2-D.

To overcome these challenges, we propose a generic LP based approach for computing precise polyhedral bounds. We demonstrate our approach for calculating a lower polyhedral

relaxation of  $h_2 = \sigma(o_2) \tanh(c_2)$ . First, we calculate the concrete intervals for two input variables via *back-substitution* [52] which is a method for computing concrete bounds on a linear expression within a region defined by the set of polyhedral constraints representable in our abstraction. It does so by recursively substituting the bounding linear expressions of target neurons with the polyhedral bounds of previous layers' neurons until reaching the input neurons. It then uses the concrete bounds of the input neurons for computing the result. In our case, the input variables are  $o_2$  and  $c_2$  and backsubstitution yields  $o_2 \in [0.4, 1.6]$  and  $c_2 \in [-0.79, 0.62]$ . We note that our abstraction can represent the affine transformations exactly. Therefore we obtain the exact interval for  $o_2 = 0.5 \cdot x + 1$  via backsubstitution whereas the obtained interval for  $c_2$  is an overapproximate one. Then, we uniformly sample a set of points  $\{(x_1, y_1), \dots, (x_n, y_n)\}$  from the input domain  $[0.4, 1.6] \times [-0.79, 0.62]$ . After it, we solve the following optimization problem to calculate the lower linear relaxation of  $h_2$ :

$$\min_{A_l, B_l, C_l \in \mathbb{R}} \sum_{i=1}^n (\sigma(x_i) \tanh(y_i) - (A_l \cdot x_i + B_l \cdot y_i + C_l)),$$

subject to the constraint that  $A_l \cdot x_i + B_l \cdot y_i + C_l \leq \sigma(x_i) \tanh(y_i)$  for each  $i$ . This is a linear program over three variables  $(A_l, B_l, C_l)$  that can be solved efficiently in polynomial time. However, the obtained bound may not be sound as the sampled points do not fully cover the continuous input domain. To address this, we shift the plane downwards by an offset (decreasing  $C_l$ ) equal to the maximum violation between  $A_l \cdot x + B_l \cdot y + C_l$  and  $h_2$ . After solving the linear program and the adjustment, we obtain  $A_l = 0.04, B_l = 0.46, C_l = 0.01$  which results in the following lower linear relaxation to  $h_2$ :  $h_2 \geq LB_{h_2} = 0.04 \cdot o_2 + 0.46 \cdot c_2 + 0.01$ . We compute the upper bound to  $h_2$ :  $h_2 \leq UB_{h_2}$  analogously.

**Comparison with prior work** Note that prior work [10] uses more expensive gradient-based optimization to obtain coefficients  $A_l, B_l, C_l$  which is orders of magnitude slower than our efficient method based on LP. Also, [53] obtain polyhedral relaxations for geometric perturbations in the image domain using LP. The difference between their method and ours is that they employ an expensive branch-and-bound based method for resolving possible unsoundness whereas we exploit the structure of non-linear operations applied in LSTMs to obtain closed-form solutions for the unsoundness in the LP solution.

After computing a linear relaxation of each neuron, we calculate the lower bound of  $h_2 - h_1$  via back-substitution. This yields:

$$\begin{aligned} \min h_2 - h_1 &\geq LB_{h_2} - UB_{h_1} \\ &\geq (0.04 \cdot o_2 + 0.46 \cdot c_2 + 0.01) - (-0.09 \cdot o_1 + 0.66 \cdot c_1 + 0.14) \\ &\geq 0.04 \cdot o_2 + 0.46 \cdot (0.07 \cdot i_2 + 0.27 \cdot g_2 + 0.09) \\ &\quad + 0.09 \cdot o_1 - 0.66 \cdot (-0.04 \cdot i_1 + 0.38 \cdot g_1 + 0.25) - 0.14 \\ &\geq 0.20 \cdot (0.5 \cdot x + 1) - 0.13 \cdot x - 0.10 \\ &\geq -0.03 \cdot x - 0.08 \geq -0.11. \end{aligned}$$

The precision of the bounds generated by our LP based method increases with the number of samples yielding optimal bounds (in the sense of small gap) asymptotically. For our example, the computed bounds are optimal. While our optimal bounds significantly improves the analysis precision compared to intervals, we still fail to certify robustness. This observation is consistent with the findings in [39], [35], [40] where it has been shown that computing suboptimal bounds can lead to better certification results for ReLU based networks. We next present our novel approach based on splitting and gradient descent that computes linear relaxations for non-linearities employed in LSTMs informed by the certification problem and proves that  $\min h_2 - h_1 > 0$  actually holds.

3) *Leveraging splitting and gradient descent*: While our method based on LP offers an efficient way to compute linear relaxations of key functions, its main limitation is that it is static as majority of previous works for neural network certification: if certification fails, there is no way to revisit the bounds and try again. In this work, we introduce a method which, upon failure of certification, makes a backward pass and adjusts the bounds to increase the precision of the verifier. Our novel approach makes the certification process more flexible to uncertified cases by seeking a combination of multiple sound bounds of the operations sufficient to verify the robustness. We start from the same back-substitution to obtain input variables' interval regions. Here, we split the original input region  $[l_x, u_x] \times [l_y, u_y]$  along two diagonals into 4 triangular regions which we denote as  $T_k$ ,  $k \in \{1, 2, 3, 4\}$ . We also set  $T_0$  equal to the full rectangular region. Next, we calculate 4 additional planes each for upper and lower bound corresponding by sampling in each subregion  $T_k$  and then applying our LP method as before. We refer to each plane as *candidate bounds*:

$$\begin{aligned} \min_{A_l, B_l, C_l \in \mathbb{R}} \sum_{i=1}^n (\sigma(x_i) \tanh(y_i) - (A_l \cdot x_i + B_l \cdot y_i + C_l)) \\ \text{subject to } \bigwedge_{i=1}^n A_l \cdot x_i + B_l \cdot y_i + C_l \leq \sigma(x_i) \tanh(y_i) \\ \text{where } (x_i, y_i) \sim T_k \end{aligned}$$

Using our LP based method, we obtain the following corresponding candidate linear relaxation for  $h_2$ ,  $LB_{h_2}^k$  for each  $T_k$  in our example:

$$\begin{aligned} h_2 &\geq LB_{h_2}^0 = 0.04 \cdot o_1 + 0.46 \cdot c_1 + 0.01 \\ h_2 &\geq LB_{h_2}^1 = 0.04 \cdot o_1 + 0.46 \cdot c_1 + 0.01 \\ h_2 &\geq LB_{h_2}^2 = 0.13 \cdot o_1 + 0.63 \cdot c_1 - 0.17 \\ h_2 &\geq LB_{h_2}^3 = 0.04 \cdot o_1 + 0.46 \cdot c_1 + 0.01 \\ h_2 &\geq LB_{h_2}^4 = 0.13 \cdot o_1 + 0.63 \cdot c_1 - 0.17 \end{aligned}$$

Note that  $LB_{h_2}^0$  denotes the linear relaxation calculated from the whole region, and there might be duplicate  $LB$ 's

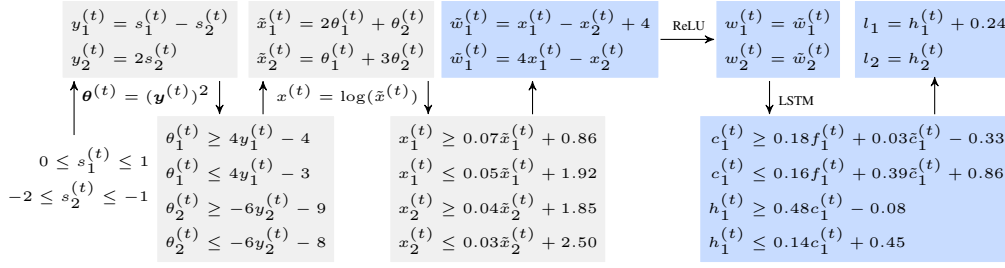


Fig. 3: Robustness certification of a speech classifier illustrated on a toy example. Each box shows the constraints computed by the verifier after processing a given operation (shown on edges). Gray color denotes the re-organized stage of speech preprocessing described in Section IV-B. Blue color denotes the network components: Affine layer, ReLU layer, LSTM and Fully Connected layer. Approximations computed with this work are shown in the bottom row. Edges without labels represent affine transformations.

when the curve in the given subregion is concave. The resulting lower bound  $LB_{h_2}$  is a linear combination of  $LB_{h_2}^k$ .

$$LB_{h_2} = \sum_{k=0}^4 \lambda_i \cdot LB_{h_2}^k, \quad \sum_{k=0}^4 \lambda_i = 1.$$

Our optimization algorithm, explained later in Section V-B, learns the values of  $\lambda_i$  via gradient descent that maximizes  $\min h_2 - h_1$ . For our example, we get  $\lambda = (0.09, 0.13, 0.34, 0.09, 0.35)$  as the set of coefficients which results in a new lower bound of  $h_2 \geq 0.10 \cdot o_2 + 0.58 \cdot c_2 - 0.11$  for the neuron  $h_2$ . We improve bounds for other neurons in similar fashion. Using the new bounds, we get  $h_2 - h_1 \geq 0.01 > 0$  which enables us to correctly certify the predicate of interest.

Compared to [10], which commit to a single bound, our method is more flexible and can tune  $\lambda$  parameters to find a combination of 5 different bounds for each neuron that yields the most precise certification result. [39], [40], [35] also suggests a similar idea of bounding ReLU's lower bound using gradient descent, but their approach is limited to the unary functions with trivial candidates. Their method is not applicable to our setting which requires handling complex binary operations having no trivial bounds from the beginning.

**Generality of our methods** Our method is generic and can be used for computing precise polyhedral bounds for the non-linearities used in LSTMs. We believe that our approach can be easily extended for obtaining polyhedral bounds for the non-linear operations in other architectures such as transformers [5] and capsule networks [54].

### B. Verifying speech classifiers

We next provide in depth demonstration of the speech classifier with various preprocessing stages and LSTM layers. The preprocessing is widely used to extract features from the raw speech signal via Mel-frequency filterbank and requires many non-linear operations. As a result, the input region to the LSTM cannot be represented as a convex set as is the case for  $L_\infty$  based perturbation on images [55]. A straightforward approach is again to overapproximate the input region via interval analysis but this results in significant imprecision as demonstrated by our experimental results in section VII. We

therefore compute a polyhedral approximation of the input region obtained after preprocessing in the same shape as used in the LSTM verifier. We next discuss the challenges involved in obtaining the polyhedral bounds.

First, the non-linear functions appearing in the stages, such as square and logarithm, are not exactly representable via linear relaxations. Both square and log functions are strictly convex and concave, respectively, so the upper bound of square and lower bound of logarithm can be calculated optimally but not the other bounds.

Also, since the domain of logarithm is positive, the verifier should never provide any negative input to the logarithm operator (negative inputs can occur due to verifier imprecision) as otherwise the analysis precision deteriorates. Computing optimal polyhedral bounds that minimize the gap can sometimes result in negative inputs to the logarithm. We therefore carefully designed our approximations for the audio preprocessing pipeline so that they are sufficiently precise and do not create negative inputs to the logarithm function. These approximations are formally presented in Section VI.

Fig. 3 shows a toy example where a single frame is fed to an LSTM based speech classifier. For the original signal with  $s_1^{(t)} = 0.5$ ,  $s_2^{(t)} = -1.5$  the output at  $l_1 > l_2$ . To prove robustness, we need to certify that the inequality holds for all signals in the region  $0 \leq s_1^{(t)} \leq 1$ ,  $-2 \leq s_2^{(t)} \leq -1$ .

Instead of showing the full process for calculating  $\min l_1 - l_2$ , we here demonstrate the computation of the lower polyhedral bound for  $x_1^{(t)}$  which is the final output of the speech preprocessing pipeline and therefore, an input of the neural network. The bounds computed for different stages of the pipeline are shown in gray parts of Fig. 3.

First, we compute the polyhedral constraints for  $y^{(t)}$ , the result of the first speech preprocessing stage which applies an affine transformation on the set of perturbed speech signals. As mentioned before, our abstraction is exact for affine transformation. Next we use back-substitution technique for calculating exact lower and upper bounds for  $y^{(t)}$ . Hence we get  $y_1^{(t)} = s_1^{(t)} - s_2^{(t)} \in [1, 3]$  and  $y_2^{(t)} = 2s_2^{(t)} \in [-4, -2]$ .

Next we calculate the lower and upper polyhedral bounds for  $\theta^{(t)} = y^{(t)} \odot y^{(t)}$ , based on the concrete bounds of

$\mathbf{y}^{(t)}$  using our method for approximating the output of the square operation defined in Section VI. We obtain following polyhedral constraints:

$$\begin{aligned} 4y_1^{(t)} - 4 &\leq \theta_1^{(t)} \leq 4y_1^{(t)} - 3 \\ -6y_2^{(t)} - 9 &\leq \theta_2^{(t)} \leq -6y_2^{(t)} - 8 \end{aligned}$$

The third stage is again an affine transformation, we handle it as for the first stage obtaining the polyhedral constraints for  $\tilde{\mathbf{x}}^{(t)}$  shown in Fig. 3. We next backsubstitution for obtaining concrete lower and upper bounds for  $\tilde{x}_1^{(t)}$  as:

$$\begin{aligned} \min \tilde{x}_1^{(t)} &= \min 2\theta_1^{(t)} + \theta_2^{(t)} \geq 2(4y_1^{(t)} - 4) + (-6y_2^{(t)} - 9) \\ &= 8(s_1^{(t)} - s_2^{(t)}) - 6(2s_2^{(t)}) - 17 \\ &= 8s_1^{(t)} - 20s_2^{(t)} - 17 \geq 3, \end{aligned}$$

Analogously, we obtain the upper bound as 34.

We use the obtained concrete bounds for calculating an overapproximation of the output of the log operation which is applied at the final stage of the pipeline. Our approximation described in section VI yields the following lower linear relaxation of  $x_1^{(t)}$ :

$$x_1^{(t)} \geq \log 3 + \frac{\tilde{x}_1^{(t)} - 3}{34 - 3} \log \frac{34}{3}$$

## V. SCALABLE CERTIFICATION OF LSTMS

In this section, we provide technical details of our method for the robustness certification of LSTM networks. In our method, we bound each neuron  $x_j$  in the network with polyhedral constraints defined over neurons from the previous layers; we have  $\sum_{i < j} a_i \cdot x_i + b \leq x_j \leq \sum_{i < j} a'_i \cdot x_i + b'$ . This abstraction is the same as the one used in [52] and allows us to exactly capture affine transformations which are frequently applied both in the speech preprocessing pipeline and neural network.

The non-linear operations applied in the LSTM cannot be exactly represented in our abstraction. Computing polyhedral bounds on their output is more challenging than for feedforward networks, as explained in section IV. In this section, we show how to obtain tight, asymptotically optimal polyhedral bounds on key operations in the LSTM unit:  $\sigma(x) \tanh(y)$  and  $\sigma(x)y$ . Then, we present a novel method to dynamically choose between different polyhedral relaxations guided by the certification problem in order to increase the precision of the certifier. In the next section, we will present our novel method for efficiently obtaining precise polyhedral bounds on the output of non-linear operations in the audio preprocessing pipeline.

### A. Computing linear relaxation of LSTM operations

Here, our goal is to bound the product of either *sigmoid and tanh* or *sigmoid and identity*, using lower and upper polyhedral planes parameterized by coefficients  $A_l, B_l, C_l$  and  $A_u, B_u, C_u$ , respectively. Let  $f(x, y) = \sigma(x) \tanh(y)$  and  $g(x, y) =$

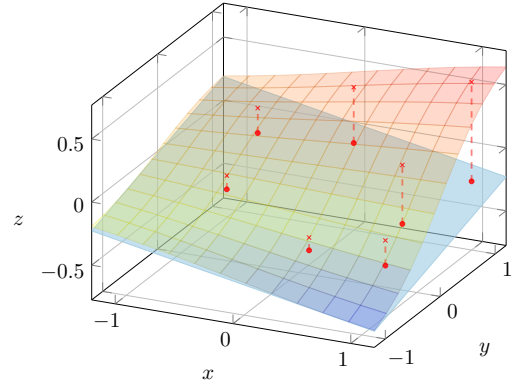


Fig. 4: Visualization of the  $z = \sigma(x) \tanh(y)$  curve and the upper bound computed by linear programming. Red crosses represent the sampled points and dashed arrows show the difference between the curve and the plane (summands in the optimization).

$\sigma(x)y$ . For  $h \in \{f, g\}$  we next provide details on calculating the lower polyhedral bound of  $h$ .

$$A_l \cdot x + B_l \cdot y + C_l \leq h(x, y) \leq A_u \cdot x + B_u \cdot y + C_u$$

We formulate the search for a lower bound of  $h(x, y)$  as an optimization problem with the aim to minimize the volume between the bound and the function, subject to the constraint that the lower bound is below the function value:

$$\begin{aligned} \min_{A_l, B_l, C_l} & \int_{(x, y) \in B} (h(x, y) - (A_l \cdot x + B_l \cdot y + C_l)) \\ \text{subject to } & A_l \cdot x + B_l \cdot y + C_l \leq h(x, y), \forall (x, y) \in B. \end{aligned} \quad (1)$$

Here, we denote  $B = [l_x, u_x] \times [l_y, u_y]$  as the boundaries of input neurons  $x$  and  $y$ . The boundaries are obtained by finding the maximum and minimum for neurons  $x$  and  $y$  with respect to the polyhedral constraints for the neurons in the previous layers using backsubstitution [52]. Prior work [10] solves this optimization problem using gradient-based methods which is both expensive and lacks convergence guarantees. Instead, we propose to solve Eq. (1) via sampling and linear programming, which is significantly faster and more precise than prior work, as we demonstrate experimentally.

**Step 1: Approximation via LP** In the first step, we solve an approximation of the intractable optimization problem from Eq. (1), obtaining potentially unsound constraints. Unsoundness implies that there can be points in region  $B$  which violate the bounds. We build on the approach from [53] which proposes to approximate the objective in Eq. (1) using Monte Carlo sampling. Let  $D = \{(x_1, y_1), \dots, (x_n, y_n)\}$  be a set of points from  $B$  sampled uniformly at random. We phrase the

following optimization problem:

$$\begin{aligned} \min_{A_l, B_l, C_l \in \mathbb{R}} \quad & \sum_{i=1}^n (h(x_i, y_i) - (A_l \cdot x_i + B_l \cdot y_i + C_l)) \\ \text{subject to} \quad & \bigwedge_{i=1}^n A_l \cdot x_i + B_l \cdot y_i + C_l \leq h(x_i, y_i). \end{aligned} \quad (2)$$

In Fig. 4 we show an input region with Monte Carlo samples as red circles and summands in the LP objective as vertical lines. As this is a linear program (LP), we can solve it exactly in polynomial time using off-the-shelf LP solvers. We compute an upper bound analogously.

**Step 2: Adjusting the offset to guarantee soundness** Since we compute the lower bound from a subset of points in  $B$ , there can be a point in  $B$  where the value of function  $h(x, y)$  is less than our computed lower bound. To ensure soundness, we compute  $\Delta_l = \max_{(x, y) \in B} h(x, y) - (A_l \cdot x + B_l \cdot y + C_l)$  and then adjust the lower bound downwards by updating the offset  $C_l \leftarrow C_l - \Delta_l$ , resulting in a sound lower bound plane. We note that the method of [53] also performs offset calculation for obtaining sound bounds however their setting is different. They perform certification of image classifiers against geometric perturbations where they use expensive branch and bound for calculating the offset. In contrast, we exploit the structure of non-linearities used in LSTMs obtaining a closed-form formula for the offset yielding an exact solution.

Next, we provide details of our offset adjustment method for  $f(x, y) = \sigma(x) \tanh(y)$  and  $g(x, y) = \sigma(x)y$ :

**Offset calculation for  $f(x, y) = \sigma(x) \tanh(y)$**  Let  $A_l \cdot x + B_l \cdot y + C_l$  be the initial lower bounding plane obtained from LP in the region  $B$ . We define  $F(x, y)$  as:

$$F(x, y) = \sigma(x) \tanh(y) - (A_l \cdot x + B_l \cdot y + C_l)$$

To find  $\Delta_l = \max_{(x, y) \in B} F(x, y)$ , we first find the extreme points by computing partial derivatives.

$$\frac{\partial F}{\partial x} = \sigma(x) \tanh(y) (1 - \sigma(x)) - A_l \quad (3)$$

$$\frac{\partial F}{\partial y} = \sigma(x) (1 - \tanh^2(y)) - B_l \quad (4)$$

We consider three cases:

- *Case 1:  $x \in \{l_x, u_x\}$*  Under this condition, we denote  $S_x := \sigma(x)$  as a constant. To ease the notation, let  $t = \tanh(y)$  where  $t \in [\tanh(l_y), \tanh(u_y)]$ . Then  $\frac{\partial F}{\partial y} \stackrel{!}{=} 0$  can be rewritten as

$$1 - t^2 = \frac{B_l}{S_x} \quad (5)$$

- *Case 2:  $y \in \{l_y, u_y\}$*  Here we set  $T_y := \tanh(y)$  and  $s = \sigma(x)$ ,  $x \in [\sigma(l_x), \sigma(u_x)]$  analogously.  $\frac{\partial F}{\partial x} \stackrel{!}{=} 0$  can be rewritten as

$$s(1 - s) = \frac{A_l}{T_y} \quad (6)$$

- *Case 3: otherwise* Otherwise, we consider both  $\frac{\partial F}{\partial x} \stackrel{!}{=} 0$  and  $\frac{\partial F}{\partial y} \stackrel{!}{=} 0$ . By combining Eq. (3) and Eq. (4), we reduce  $\tanh(y)$  and obtain

$$s^4 + (-2 - B_l)s^3 + (1 + 2B_l)s^2 + (-B_l)s - A_l^2 \stackrel{!}{=} 0 \quad (7)$$

We note that  $F(x, y)$  is differentiable and the region  $B$  is compact, by Fermat's theorem  $F$  achieves its maximum at either the roots of Eq. (5), Eq. (6), and Eq. (7), or the 4 corner coordinates of  $B$ . We evaluate  $F$  at these points to get  $\Delta_l$ . By replacing  $C_l \leftarrow C_l - \Delta_l$ , modified  $F$  is no greater than 0, which means the plane is always equal or strictly below the  $\sigma(x) \tanh(y)$  curve.

**Offset calculation for  $g(x, y) = \sigma(x)y$**  We next show offset calculation for  $\sigma(x)y$ . We define the differentiable function  $G(x, y) = \sigma(x)y - (A_l \cdot x + B_l \cdot y + C_l)$  over the compact set  $B$  and compute:

$$\frac{\partial G}{\partial x} = \sigma(x)y(1 - \sigma(x)) - A_l \quad (8)$$

$$\frac{\partial G}{\partial y} = \sigma(x) - B_l \quad (9)$$

We use Fermat's theorem and consider three cases:

- *Case 1:  $x \in \{l_x, u_x\}$*  When  $\sigma(x)$  is fixed, Eq. (9) is constant, which means  $G$  is monotonous in this case.
- *Case 2:  $y \in \{l_y, u_y\}$*  Denote  $s = \sigma(x)$  where  $s \in [\sigma(l_x), \sigma(u_x)]$ , then setting Eq. (8)  $\stackrel{!}{=} 0$  becomes

$$s(1 - s) = \frac{A_l}{y} \quad (10)$$

- *Case 3: otherwise* If there is a local extremum in the region, Hessian of  $G$  must be either positive-definite or negative-definite.

$$\frac{\partial^2 G}{\partial x^2} = \sigma(x)y(1 - \sigma(x))(1 - 2\sigma(x))$$

$$\frac{\partial^2 G}{\partial y^2} = 0$$

$$\frac{\partial^2 G}{\partial x \partial y} = \sigma(x)(1 - \sigma(x))$$

$$\frac{\partial^2 G}{\partial x^2} \cdot \frac{\partial^2 G}{\partial y^2} - \left( \frac{\partial^2 G}{\partial x \partial y} \right)^2 = -(\sigma(x)(1 - \sigma(x)))^2 < 0$$

Hence, there is no local maximum inside the boundaries. To summarize, we only need to consider the roots of the Eq. (10) and the 4 corners to calculate the maximum of  $G$  to get  $\Delta_l$  for  $\sigma(x)y$ .

We also update the upper bound analogously. Fig. 4 shows the upper bound plane obtained after solving the LP and adjusting the offset.

**Asymptotic Optimality of the sampled boundings** Finally, we can prove that, similarly to [53], as we increase the number of samples  $n$ , the solution of the LP asymptotically approaches the solution of the original problem from Eq. (1). Rephrasing and simplifying the theorem from [53]:

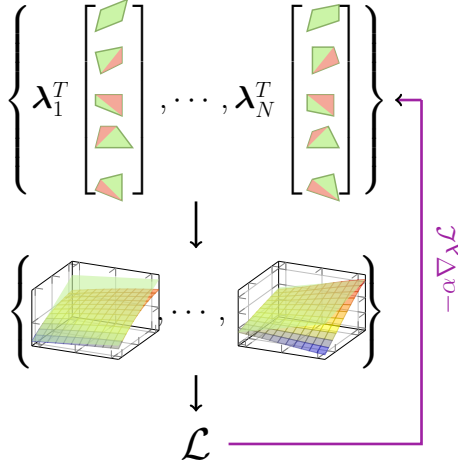


Fig. 5: Learning to combine linear bounds via gradient descent. Here the 5 candidate planes multiplied by  $\lambda$  are depicted either in green or red, or both. Green represents the sampled domain,  $T_k$ , and red is the extension of the obtained green plane out of the domain. With the linear combination of the planes, we compute the bound, calculate the loss, and backpropagate.

**Theorem 1.** Let  $N$  be the number of points sampled in the algorithm. Let  $(\omega_l, b_l)$  be our lower constraint (linear constraints and bias, respectively) and let  $L(\omega^*, b^*)$  be the true minimum of function  $L$ . For every  $\delta > 0$  there exists  $N_\delta$  such that  $|L(\omega_l, b_l) - L(\omega^*, b^*)| < \delta$  for every  $N > N_\delta$ , with high probability. Analogous result holds for upper constraint  $(\omega_u, b_u)$  and function  $U$ .

where, roughly saying,  $L = \int_{(x,y)} F(x, y)$  and analogous for the upper bound case  $U$ , and  $(\omega_l, b_l)$  are our  $A_l, B_l, C_l$ . Following the theorem, our sampling method guarantees the asymptotic optimality of our bounds.

### B. Optimizing the combination of bounds

While our approach based on sampling, linear programming and offset adjustment allow us to obtain an (asymptotically) optimal lower bound plane, it still has a fundamental limitation that it produces a *single* lower bound plane. Although the lower bound plane from Section V-A is optimal in terms of volume, this approach is, in a sense, greedy: when considering the *entire* network, it is possible that we can select non-optimal planes for each neuron, which yield more precise result in the end. Neither the method from [10] nor our method from Section V-A can achieve this – we now present the first approach which can learn how to select bounds for the entire network so as to increase end-to-end precision of the certification.

#### Step 1: Compute a set of candidate bounds

In the first step, we adapt our approach from Section V-A to produce a diverse set of candidate planes instead of a single plane. At a high level, we are going to run our Monte Carlo sampling procedure several times, each time on a different subregion of the original region  $B = [l_x, u_x] \times [l_y, u_y]$  with the

constraints still enforced over the entire region  $B$ . We define 4 different triangular subdomains:  $T_1$  and  $T_2$  are triangles resulting from splitting  $B$  along the main diagonal, while  $T_3$  and  $T_4$  are triangles resulting from splitting  $B$  along the other diagonal. We additionally define  $T_0 = B$ .

Now, for each  $k \in \{0, 1, 2, 3, 4\}$ , we perform sampling and optimization as in Eq. (2), this time sampling from  $T_k$ :

$$\begin{aligned} \min_{A_l, B_l, C_l \in \mathbb{R}} \quad & \sum_{i=1}^n (\sigma(x_i) \tanh(y_i) - (A_l \cdot x_i + B_l \cdot y_i + C_l)) \\ \text{subject to} \quad & \bigwedge_{i=1}^n A_l \cdot x_i + B_l \cdot y_i + C_l \leq \sigma(x_i) \tanh(y_i) \\ \text{where} \quad & (x_i, y_i) \sim T_k \end{aligned}$$

Additionally, for each  $k$  we also enforce the constraints at all the corners of  $B$ . For each neuron  $i$ , this yields 5 candidate lower bound and upper bound planes,  $LB_i^k$  and  $UB_i^k$  for  $k \in \{0, 1, 2, 3, 4\}$ . These 5 candidate planes for each of the  $N$  neurons are shown in Fig. 5.

#### Step 2: Find the optimal combinations of the bounds

After computing a set of candidate bounds, in the next step our goal is to learn a linear combination of these bounds which yields the highest end-to-end certification precision. To do this, we define lower and upper bound of neuron  $i$  as a linear combination of the proposed 5 bounds:

$$\begin{aligned} LB_i &= \sum_{k=0}^4 \lambda_i^{LB} \cdot LB_i^k, \quad \sum_{k=0}^4 \lambda_i^{LB} = 1, \\ UB_i &= \sum_{k=0}^4 \lambda_i^{UB} \cdot UB_i^k, \quad \sum_{k=0}^4 \lambda_i^{UB} = 1. \end{aligned}$$

Recall that we formulate robustness certification as proving that for all labels  $i$  different from the ground truth label  $t$ :

$$z_t - z_i > 0$$

Here, the lower bound on  $z_t - z_i$  is computed using back-substitution [52], as shown in our overview example in Section IV. However, this lower bound now depends on the coefficients  $\lambda$ , so we define function  $f(x, \epsilon, i, \lambda)$  which computes the lower bound of the expression  $z_t - z_i$  when using  $\lambda$  to combine the neuron bounds.

We describe our approach to find the best coefficients  $\lambda$  in Algorithm 1. Consider the number of possible labels  $m$  and the number of binary operations of interest  $N_{ops}$ . In order to find  $\lambda$ , we solve the following optimization problem for each label  $i$ :

$$z_t - z_i > \max_{\lambda} f(x, \epsilon, i, \lambda)$$

If the solution to the above optimization problem is positive, then we have established robustness with respect to the class  $i$ . First, we initialize  $\tilde{\lambda}$ , pre-normalized vector of  $\lambda$ , for each neuron uniformly between -1 and 1. Then, in each epoch we compute the normalized  $\lambda$  by applying softmax to  $\tilde{\lambda}$  and then run the certification using  $\lambda$ , obtaining loss  $\mathcal{L}$  equal to the value  $-f(x, \epsilon, i, \lambda)$ . We then perform gradient descent update

---

**Algorithm 1** Learning  $\lambda$  via gradient descent
 

---

**Given** input  $x$ , label  $y$ , model  $\mathcal{M}$ , perturbation  $\epsilon$   
 Initialize the polyhedral relaxations and candidate bounds based on  $x$ ,  $\mathcal{M}$  and  $\epsilon$ .  
**for**  $i \leftarrow 1$  **to**  $m$  **where**  $i \neq y$  **do**  
   Initialize  $\tilde{\lambda} \sim [-1, 1]^{N_{ops} \times 5}$ .  
    $epoch \leftarrow 0$   
   **repeat**  
      $\lambda \leftarrow \text{SoftMax}(\tilde{\lambda})$   
      $\mathcal{L} \leftarrow -f(x, \epsilon, i, \lambda)$   
      $\tilde{\lambda} \leftarrow \tilde{\lambda} - \alpha \nabla_{\tilde{\lambda}} \mathcal{L}$   
      $epoch \leftarrow epoch + 1$   
   **until**  $epoch = \text{max\_epoch}$  or  $\mathcal{L} < 0$   
   **if**  $\mathcal{L} \geq 0$  **then**  
     **return** not certified  
   **end if**  
**end for**  
**return** certified

---

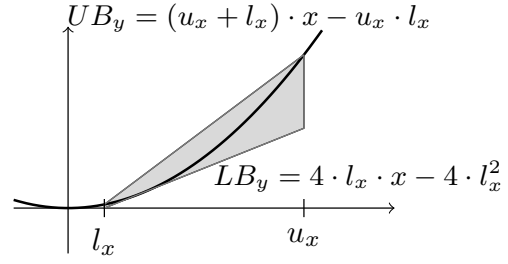
on  $\tilde{\lambda}$  based on the loss. If at some point the loss is negative, it means we have just found  $\lambda$  which enables us to prove robustness and the algorithm terminates. The core updating flow is also shown visually in Fig. 5.

Note that, although we use gradient-based methods in certification as [10], the ideas are fundamentally different: in terms of runtime, we apply the optimization for each label which is typically at most the number of output classes, while they optimize for each  $\sigma(x) \tanh(y)$  operation which is too expensive for networks as the number of neurons is typically orders of magnitude larger than the number of output classes. Further, we use optimization to adjust the bounds, while they use it to obtain a single bound, which produces worse results than our method from Section V-A as demonstrated experimentally in section VII.

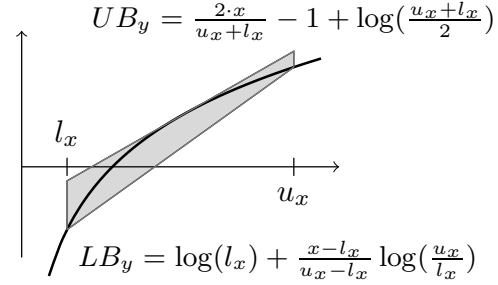
## VI. CERTIFICATION OF SPEECH PREPROCESSING

We demonstrate the scalability of our approach by certifying, for the first time, the robustness of a speech classifier based on LSTMs. The speech preprocessing pipeline transforms the original set of perturbed speech signals, represented as a set of interval constraints, through complex operations into a non-linear and non-convex set. Propagating the resulting set through the network is computationally expensive. We therefore obtain a precise overapproximation of this set in the polyhedral abstraction used in section V for verifying LSTMs. This abstraction yields more precise certification results than computing an interval approximation of the LSTM input set and then propagating the result through our polyhedral LSTM verifier. We next present our new efficient methods for computing the polyhedral approximation of the output of the speech preprocessing pipeline.

The first and third stages of the pipeline described in Section IV involve an affine transformation which is captured exactly using our abstraction. We next introduce our polyhedral relaxations for the stages involving the application of the



(a) Linear relaxation for square function with threshold  $\delta = 0$



(b) Linear relaxation for log function.

Fig. 6: Two relaxations for the speech preprocessing stage.

Square and Log operations. We provide closed form formulas for the polyhedral bounds based on the concrete lower and upper bounds of the inputs, computed using backsubstitution. As a result, these can be computed in constant time.

### A. Square

The lower and upper polyhedral bounds of the output of the square function  $y = x^2$  where  $x \in [l_x, u_x]$  are shown in Fig. 6a. We first consider the bounds for  $y$  which minimize the area in the  $xy$ -plane. The upper bound  $UB_y$  is obtained by computing the chord joining the end points  $(l_x, l_x^2)$  and  $(u_x, u_x^2)$ . The lower bound is a line parallel to  $UB_y$  passing through a point  $((u_x + l_x)/2, ((u_x + l_x)/2)^2)$  in the middle of the curve.

$$LB_y = (u_x + l_x) \cdot x - ((u_x + l_x)/2)^2$$

$$UB_y = (u_x + l_x) \cdot x - u_x \cdot l_x.$$

While the above bounds would be sufficient in any other domain, they do not work for the speech domain as the subsequent Log requires that the input be strictly non-negative as it is not defined for negative inputs. Taking these constraints into account, we obtain the following lower and upper polyhedral bounds:

$$LB_y = \begin{cases} 4 \cdot l_x \cdot x - 4 \cdot l_x^2 & 0 \leq l_x < u_x/3 \\ 4 \cdot u_x \cdot x - 4 \cdot u_x^2 & 0 \geq 3 \cdot u_x > l_x \\ 0 & l_x \leq 0 \leq u_x \\ (u_x + l_x) \cdot x - ((u_x + l_x)/2)^2 & o.w. \end{cases}$$

$$UB_y = (u_x + l_x) \cdot x - u_x \cdot l_x.$$

This design of linear relaxations minimizes the area between the bounds and the  $x$  region while they satisfy the non-negativity. However, due to floating point errors in computing divisions during runtime for inputs around zero might create the violation of the range constraint. Hence, we parametrize our relaxation with  $\delta \in \mathbb{R}$ , a small threshold value to ensure that the lower bound stays non-negative. In our experiments, we set  $\delta = 1 \times 10^{-5}$ . Our final lower and upper polyhedral bounds for  $y = x^2$  can be computed as:

$$LB_y = \begin{cases} 2 \cdot (l_x + \sqrt{l_x^2 - \delta}) \cdot x & 3 \cdot l_x^2 + 2 \cdot l_x \cdot u_x - u_x^2 \\ \quad - (l_x + \sqrt{l_x^2 - \delta})^2 & \leq 4 \cdot \delta, \quad \sqrt{\delta} \leq l_x \\ 2 \cdot (u_x - \sqrt{u_x^2 - \delta}) \cdot x & 3 \cdot u_x^2 + 2 \cdot u_x \cdot l_x - l_x^2 \\ \quad - (u_x - \sqrt{u_x^2 - \delta})^2 & \leq 4 \cdot \delta, \quad u_x \leq -\sqrt{\delta} \\ 0 & l_x \leq \sqrt{\delta}, -\sqrt{\delta} \leq u_x \\ (u_x + l_x) \cdot x - & \\ \quad ((u_x + l_x)/2)^2 & o.w. \end{cases}$$

$$UB_y = (u_x + l_x) \cdot x - u_x \cdot l_x.$$

### B. Log

We next provide polyhedral relaxation of the output  $y = \log(x)$  of the log operation where  $x \in [l_x, u_x]$ , shown in Fig. 6b. Our relaxations are optimal and minimize the area in the  $xy$ -plane. The lower bound  $B_y$  can be obtained by computing the chord joining the end points  $(l_x, \log(l_x))$  and  $(u_x, \log(u_x))$ . The upper bound  $UB_y$  is obtained by computing a line parallel to  $LB_y$  passing through the middle of the curve at  $((u_x + l_x)/2, \log((u_x + l_x)/2))$ .

Our final relaxations can be computed as:

$$LB_y = \log(l_x) + \frac{x - l_x}{u_x - l_x} \log\left(\frac{u_x}{l_x}\right)$$

$$UB_y = \frac{2 \cdot x}{u_x + l_x} - 1 + \log\left(\frac{u_x + l_x}{2}\right).$$

## VII. EXPERIMENTAL EVALUATION

We now evaluate the effectiveness of our approach for certifying the robustness of LSTM networks.

**Setup** We implemented R2 in PyTorch [56] and used Gurobi 9.0 to solve linear programs. All the experiments except the ones with Google Speech Commands (GSC) dataset were performed on a single Tesla V100 whereas the GSC experiments were run on an Nvidia GeForce RTX 2080. Following convention from prior work [52], we consider only those inputs that were correctly classified without perturbation. We use the same set of hyperparameters for the experiments unless specifically mentioned. We use 100 sampling points for constructing the linear program and optimize  $\lambda$  parameters using Adam [57] for 100 epochs. During optimization, we initialize the learning rate to 100 and multiply it by 0.98 after every epoch.

### A. Image classification

We first evaluate R2 on the image classification task proposed by [10]. They use the MNIST dataset [58] and flatten each image into a vector of dimension 784. Then, this vector

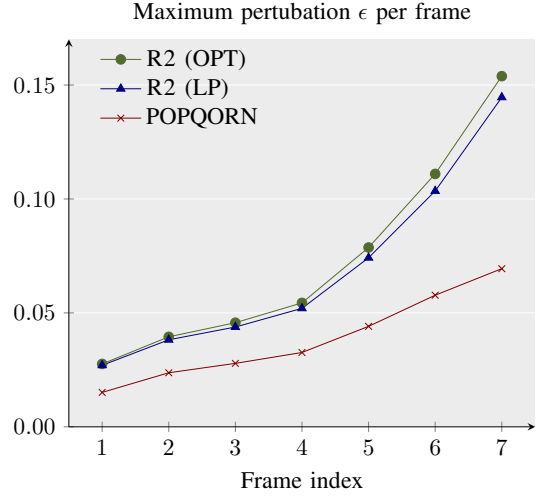


Fig. 7: Results for the comparison between R2 and POPQORN. Plotted points represent the maximum  $L_\infty$  norm perturbation for each frame index 1 through 7.

is partitioned into a sequence of  $f$  frames ( $f$  depends on the experiment). This frame sequence is then used as an input to the LSTM.

**Comparison with POPQORN** We now compare precision and scalability of R2 with POPQORN [10]. We closely follow the evaluation setup used in the experiments of [10]. We trained an LSTM network containing 1 layer with 32 hidden units using standard training achieving an accuracy of 96.5%. The network receives a sequence of  $f = 7$  image slices as input and predicts a digit corresponding to the image. We evaluate three methods: POPQORN [10], our first method based on sampling and linear programming from Section V-A, denoted as R2 (LP), and our second method based on optimization of the bounds from Section V-B, denoted as R2 (OPT). Note that OPT also uses LP as its subroutine, as explained in Section V-B.

As POPQORN is slow, we evaluate this experiment only on 10 correctly classified images randomly sampled from the test set. For each frame index  $i$  and each method, we compute the maximum  $\epsilon$  such that the method can certify that LSTM is robust to perturbations up to  $\epsilon$  in the  $L_\infty$ -norm of the  $i$ -th slice of the image. For each method, we compute this maximum  $\epsilon$  that can be certified using the same binary search procedure as in [10].

We show the results of this experiment in Fig. 7. First, we observe that perturbations in early frames allow us to certify much smaller  $\epsilon$  than that in later frames. This is because the approximation error on frame 1 propagates through the later frames to the classifying layer while the error on frame 7 only affects the last layer. Across all frames, both our methods, LP and OPT, significantly outperform POPQORN. We can also see that OPT which can dynamically adjust the bounds can prove more than LP, which uses fixed single linear relaxation per neuron.

We next compare running times of the three methods on

$F$	$H$	$L$	Accuracy(%)	Certified(%) by OPT / LP	Running time(s) by OPT
4	32	1	96.1	91.0 / 89.0	14.55
4	32	2	96.7	92.0 / 73.0	29.17
4	32	3	95.8	95.0 / 65.0	43.10
4	64	1	97.3	93.0 / 92.0	27.03
4	128	1	97.1	95.0 / 95.0	52.40
7	32	1	96.5	63.0 / 56.0	32.19

Table I: Certification of several LSTM models using R2.  $F$ ,  $H$ , and  $L$  in the label stands for a model consisting of  $F$  frames,  $H$  hidden units in an LSTM cell, and  $L$  layers in the LSTM, respectively. All experiments were run with  $\epsilon = 0.010$ .

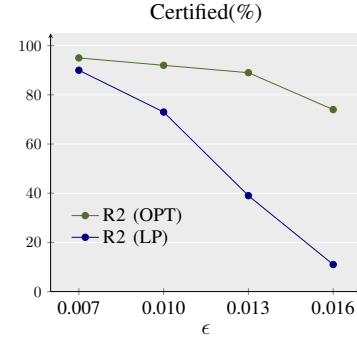
perturbations in the first frame – most challenging as it requires propagating through all timesteps. Here, R2 (LP) takes 65 seconds, R2 (OPT) takes 348 seconds and POPQORN takes 2160 seconds per example on average. Based on this, we conclude that both variants of R2 are more precise than POPQORN while being  $33.2\times$  (for LP) and  $6.21\times$  more scalable (for OPT).

**Comparison against POPQORN combined with hash tables** One way to make the prior work POPQORN more scalable by using a hash table. The idea here is to store the coefficients of the bounding planes approximating the binary functions computed by POPQORN in the table indexed by the intervals  $[l_x, u_x]$  and  $[l_y, u_y]$  of the input variables  $x$  and  $y$ . For our benchmarks both  $x$  and  $y$  are usually in the range  $[-2, 2]$ . The keys  $l_x, u_x, l_y, u_y$  in the table are such that  $l_x, u_x, l_y, u_y, u_x - l_x$  and  $u_y - l_y$  are all divisible by a constant  $\delta \in \mathbb{R}$ . The coefficients for any missing entry  $[l'_x, u'_x], [l'_y, u'_y]$  in our table is obtained by finding the smallest intervals in the table  $[l_x, u_x], [l_y, u_y]$  containing  $[l'_x, u'_x]$  and  $[l'_y, u'_y]$  respectively. Our construction ensures that such intervals always exist.

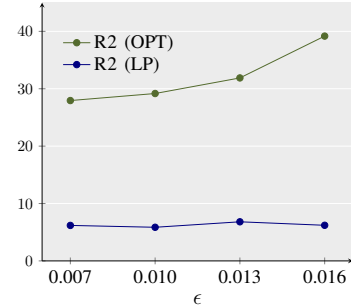
While this approach speeds up POPQORN, it comes at a cost of extra memory and loss of precision in practice. There are already 672,400 different cases within the domain  $[-2, 2] \times [-2, 2]$  with  $\delta = 0.1$  which significantly increases memory footprint. Decreasing the value of  $\delta = 0.01$  improves the precision of the combination but also exponentially increases the size of the table making it computationally prohibitive. The drop in the precision of certification is noticeable: POPQORN proves 79.2% out of 500 test data perturbed at frame 7 with  $\epsilon = 0.05$  while combining it with hash table proves 76.0%. We note that in comparison the  $\epsilon$  values for every frame proven by R2 are almost twice as large as for POPQORN.

**Performance demonstration with various model sizes** In this experiment, we evaluate the scalability of R2 by certifying several recurrent architectures, with varying number of frames  $F$ , hidden units  $H$  and LSTM layers  $L$ . For each network, we certify the first 100 correctly classified images using the same perturbation  $\epsilon = 0.01$  for all frames, with 3 repetitions. While in the previous experiment we certified each frame separately to closely follow the setup from [10], it is more natural to assume the adversary is able to perturb the entire input.

We show our results in Table I. Here we first observe that



(a) MNIST precision



(b) MNIST runtime

Fig. 8: Performance plots of MNIST dataset with different epsilons. All tests are done with 04F\_032H\_2L.

the precision of R2 is affected mostly by the number of frames as the precision loss accumulates along the frames. Naturally, running time increases with the number of neurons and frames, as R2 is optimizing the bounds for each  $\sigma(x) \tanh(y)$  operation.

However, we also observe a counter-intuitive phenomenon that R2 (OPT) performs better with multiple-layers models than the single-layer model. The precisions from R2 (LP) drops with increasing the number of LSTM layers increase unlike those from R2 (OPT). Our hypothesis is that an increased number of trainable parameters enhances the flexibility of the bounds for the optimization, allowing us to find more combinations of the bounds which allow certification of the input. R2 (LP) has non-flexible bounds, so the error simply propagates through the layers.

We also tried to plug-in the POPQORN bounds, but it results in precision of 83% and takes an average of 1150 sec per input, even for our smallest model, 04F\_032H\_1L. As shown in Table I, R2 proves 91.0% for the same model in 14.55 seconds.

**Performance demonstration with increasing perturbation** In the next experiment, we certify robustness of the MNIST classifier for different  $\epsilon$  values. We evaluated on 100 correctly classified samples from the test set and the show the results in Fig. 8. R2 significantly improves the precision: for example for  $\epsilon = 0.013$  in Fig. 8a, LP proves 39% while OPT certifies 89% of samples. These results confirm that learning

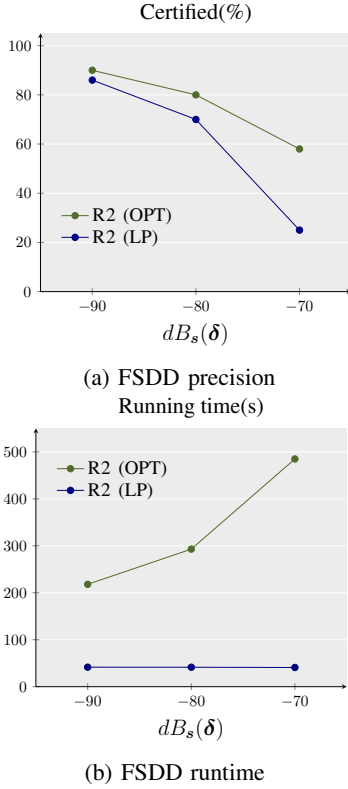


Fig. 9: Performance plots of FSDD dataset with different dB perturbation. All tests are done with the same architecture described in the text.

the bounds dynamically has a large impact on certification precision. In terms of runtime shown in Fig. 8b, OPT naturally consumes more time than LP, but this is justified by the significant increase in precision.

### B. Speech classification

In the next experiment, we certify robustness of a speech classifier on the FSDD dataset [59] and GSC dataset v2 [45]. FSDD consists of recordings of digits spoken by 6 different speakers, recorded at 8kHz. and GSC has 35 different labels of single word utterances in 16kHz. Unlike the MNIST task, these tasks are more challenging for LSTM certification as the speech signal is naturally a time series data with variable length. As POPQORN does not handle speech preprocessing and is too slow for handling long speech signals, we evaluated only our methods.

**Preprocessing** As mentioned before, one of the key challenges in speech classification, not encountered in the vision domain, is the presence of a complex preprocessing stage before the input is passed to the LSTM network. The preprocessing stage in this experiment consists of FFT and Mel-filter transformations. Preprocessed input is then passed through the fully connected layer with ReLU activation, and then through the LSTM unit.

**Certifying FSDD classifier** We used the following parameters for the preprocessing: we slice the raw wav signal with

length 256 using a step size 200 with 10 Mel-frequencies. For this experiment, we trained an LSTM network with two LSTM layers and 32 hidden units, preceded by a 40 ReLU-activated fully-connected layer. This network achieves accuracy of 83.6% on the FSDD task. The average number of frames was 14.7, which is more than double compared to the previous task on the MNIST dataset.

Our perturbation metric on speech classification tasks is described in Section III-A. We show our results in Fig. 9. We vary the decibel perturbation between -90 dB and -70 dB and evaluate the precision and runtime of R2. Fig. 9a shows percentage of certified samples: our method based on optimizing the bounds (OPT) performs best, e.g., certifying more than two times than LP for a significant perturbation of -70 dB. In terms of runtime, Fig. 9b shows that the OPT runtime increases with the perturbation magnitude, meaning that the optimizer needs more iterations to converge to the resulting bounds.

**Precision boost with polyhedral approximations of speech preprocessing** We also conducted an additional experiment to show the importance of designing proper polyhedral relaxation of the speech preprocessing pipeline. We replaced the polyhedral bounds for both square and logarithm operations with interval constraints, the precision of R2 (LP) dropped to 61% on -90dB and 20% on -80dB. The corresponding precision with polyhedral bounds are 86% and 70%, respectively. This shows the importance of keeping relational information while overapproximating the speech preprocessing pipeline.

**Certifying GSC classifier** We used the following parameters for the preprocessing: we downsample the raw input to 8kHz, sliced the signal in length 1024, followed by 10 Mel-frequency filterbanks. As with FSDD architecture, we used two layers of LSTM and 50 hidden units, preceded by a 50 ReLU-activated fully-connected layer. This network achieves accuracy of 80% on the GSC task.

Certifying GSC classifier is especially more challenging than the previous tasks. This dataset has 35 labels, which is significantly more than the 10 labels in both MNIST and FSDD. The larger label set size requires R2 to compare 34 logit differences - acquiring the lower bounds of  $l_{GT} - l_{FL}$  where each term stands for the final logit for the ground truth and false label, respectively.

We show our results in Fig. 10. Fig. 10a shows percentage of certified samples: 75% on -110dB and 46% on -100dB with R2 (OPT), again larger precisions than R2 (LP). Fig. 10b shows longer running time for R2 (OPT) than on other datasets. This is due to the larger label set size of GSC.

## VIII. CONCLUSION

We presented a novel approach for certifying recurrent neural networks based on a combination of linear programming and optimization. The key idea was to compute a convex relaxation of the non-linear operations found in the recurrent cells and to be able to dynamically adjust this relaxation according to each input example being certified.

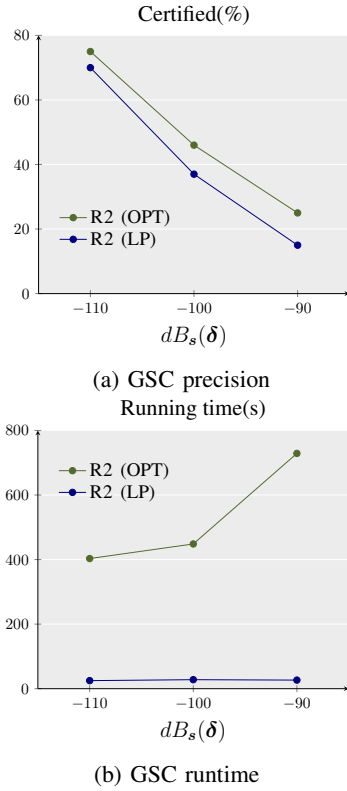


Fig. 10: Performance plots of GSC dataset with different dB perturbation. All tests are done with the same architecture described in the text.

Our experimental results indicate that R2 is both more precise and more scalable than prior work, while offering guarantees on convergence. Thanks to these advances, using R2, we were able to certify, for the first time, the robustness of LSTMs used in speech recognition.

## REFERENCES

- [1] N. Papernot, P. McDaniel, A. Swami, and R. Harang, "Crafting adversarial input sequences for recurrent neural networks," in *MILCOM 2016-2016 IEEE Military Communications Conference*. IEEE, 2016, pp. 49–54.
- [2] N. Carlini and D. Wagner, "Audio adversarial examples: Targeted attacks on speech-to-text," in *2018 IEEE Security and Privacy Workshops (SPW)*, 2018.
- [3] J. Li, S. Qu, X. Li, J. Szurley, J. Z. Kolter, and F. Metzger, "Adversarial music: Real world audio adversary against wake-word detection system," in *Advances in Neural Information Processing Systems*, 2019, pp. 11 908–11 918.
- [4] W. Hu and Y. Tan, "Black-box attacks against rnn based malware detection algorithms," *arXiv preprint arXiv:1705.08131*, 2017.
- [5] A. Vaswani, N. Shazeer, N. Parmar, J. Uszkoreit, L. Jones, A. N. Gomez, L. u. Kaiser, and I. Polosukhin, "Attention is all you need," in *Proc. Neural Information Processing Systems (NIPS)*, I. Guyon, U. V. Luxburg, S. Bengio, H. Wallach, R. Fergus, S. Vishwanathan, and R. Garnett, Eds., 2017, pp. 5998–6008.
- [6] P. Filonov, A. Lavrentyev, and A. Vorontsov, "Multivariate industrial time series with cyber-attack simulation: Fault detection using an lstm-based predictive data model," *arXiv preprint arXiv:1612.06676*, 2016.
- [7] A. Diro and N. Chilamkurti, "Leveraging lstm networks for attack detection in fog-to-things communications," *IEEE Communications Magazine*, vol. 56, no. 9, pp. 124–130, 2018.

- [8] J. Pachocki, G. Brockman, J. Raiman, S. Zhang, H. Pondé, J. Tang, F. Wolski, C. Dennison, R. Jozefowicz, P. Debiak *et al.*, "Openai five," URL <https://blog.openai.com/openai-five>, 2018.
- [9] O. Vinyals, I. Babuschkin, J. Chung, M. Mathieu, M. Jaderberg, W. M. Czarnecki, A. Dudzik, A. Huang, P. Georgiev, R. Powell *et al.*, "Alphastar: Mastering the real-time strategy game starcraft ii," *DeepMind blog*, p. 2, 2019.
- [10] C. Ko, Z. Lyu, T. Weng, L. Daniel, N. Wong, and D. Lin, "Popqorn: Certifying robustness of recurrent neural networks," in *International Conference on Machine Learning (ICML)*, 2019.
- [11] C. Szegedy, W. Zaremba, I. Sutskever, J. Bruna, D. Erhan, I. Goodfellow, and R. Fergus, "Intriguing properties of neural networks," *arXiv preprint arXiv:1312.6199*, 2013.
- [12] B. Biggio, I. Corona, D. Maiorca, B. Nelson, N. Šrđić, P. Laskov, G. Giacinto, and F. Roli, "Evasion attacks against machine learning at test time," in *Joint European conference on machine learning and knowledge discovery in databases*, 2013.
- [13] N. Carlini, P. Mishra, T. Vaidya, Y. Zhang, M. Sherr, C. Shields, D. Wagner, and W. Zhou, "Hidden voice commands," in *25th {USENIX} Security Symposium ({USENIX} Security 16)*, 2016, pp. 513–530.
- [14] A. Hannun, C. Case, J. Casper, B. Catanzaro, G. Diamos, E. Elsen, R. Prenger, S. Satheesh, S. Sengupta, A. Coates *et al.*, "Deep speech: Scaling up end-to-end speech recognition," *arXiv preprint arXiv:1412.5567*, 2014.
- [15] Y. Qin, N. Carlini, I. Goodfellow, G. Cottrell, and C. Raffel, "Imperceptible, robust, and targeted adversarial examples for automatic speech recognition," in *International Conference on Machine Learning (ICML)*, 2019.
- [16] P. Neekhar, S. Hussain, P. Pandey, S. Dubnov, J. McAuley, and F. Koushanfar, "Universal adversarial perturbations for speech recognition systems," *arXiv preprint arXiv:1905.03828*, 2019.
- [17] Z. Yang, B. Li, P.-Y. Chen, and D. Song, "Characterizing audio adversarial examples using temporal dependency," 2019.
- [18] G. Katz, C. Barrett, D. L. Dill, K. Julian, and M. J. Kochenderfer, "Reluplex: An efficient smt solver for verifying deep neural networks," in *International Conference on Computer Aided Verification*. Springer, 2017, pp. 97–117.
- [19] T. Gehr, M. Mirman, D. Drachler-Cohen, P. Tsankov, S. Chaudhuri, and M. Vechev, "Ai2: Safety and robustness certification of neural networks with abstract interpretation," in *2018 IEEE Symposium on Security and Privacy (SP)*. IEEE, 2018, pp. 3–18.
- [20] G. Singh, T. Gehr, M. Mirman, M. Püschel, and M. T. Vechev, "Fast and effective robustness certification," in *Advances in Neural Information Processing Systems (NeurIPS)*, 2018.
- [21] W. Ruan, X. Huang, and M. Kwiatkowska, "Reachability analysis of deep neural networks with provable guarantees," in *Proc. International Joint Conference on Artificial Intelligence, IJCAI*, 2018, pp. 2651–2659.
- [22] H. Zhang, T. Weng, P. Chen, C. Hsieh, and L. Daniel, "Efficient neural network robustness certification with general activation functions," in *Advances in Neural Information Processing Systems (NeurIPS)*, 2018.
- [23] T. Weng, H. Zhang, H. Chen, Z. Song, C. Hsieh, L. Daniel, D. S. Boning, and I. S. Dhillon, "Towards fast computation of certified robustness for relu networks," in *International Conference on Machine Learning (ICML)*, 2018.
- [24] H. Salman, G. Yang, H. Zhang, C. Hsieh, and P. Zhang, "A convex relaxation barrier to tight robustness verification of neural networks," in *Advances in Neural Information Processing Systems (NeurIPS)*, 2019.
- [25] G. Singh, R. Ganvir, M. Püschel, and M. Vechev, "Beyond the single neuron convex barrier for neural network certification," in *Advances in Neural Information Processing Systems*, 2019.
- [26] S. Wang, K. Pei, J. Whitehouse, J. Yang, and S. Jana, "Formal security analysis of neural networks using symbolic intervals," in *27th {USENIX} Security Symposium ({USENIX} Security 18)*, 2018, pp. 1599–1614.
- [27] A. Raghunathan, J. Steinhardt, and P. S. Liang, "Semidefinite relaxations for certifying robustness to adversarial examples," in *Advances in Neural Information Processing Systems (NeurIPS)*, 2018.
- [28] S. Wang, K. Pei, J. Whitehouse, J. Yang, and S. Jana, "Efficient formal safety analysis of neural networks," in *Advances in Neural Information Processing Systems*, 2018, pp. 6367–6377.
- [29] G. Singh, T. Gehr, M. Püschel, and M. Vechev, "Boosting robustness certification of neural networks," in *International Conference on Learning Representations*, 2019.

- [30] E. Wong and J. Z. Kolter, "Provable defenses against adversarial examples via the convex outer adversarial polytope," *arXiv preprint arXiv:1711.00851*, 2017.
- [31] A. Raghunathan, J. Steinhardt, and P. Liang, "Certified defenses against adversarial examples," in *International Conference on Learning Representations*, 2018.
- [32] M. Mirman, T. Gehr, and M. Vechev, "Differentiable abstract interpretation for provably robust neural networks," in *International Conference on Machine Learning*, 2018, pp. 3575–3583.
- [33] S. Gowal, K. Dvijotham, R. Stanforth, R. Bunel, C. Qin, J. Uesato, T. Mann, and P. Kohli, "On the effectiveness of interval bound propagation for training verifiably robust models," *arXiv preprint arXiv:1810.12715*, 2018.
- [34] H. Zhang, H. Chen, C. Xiao, S. Gowal, R. Stanforth, B. Li, D. Boning, and C.-J. Hsieh, "Towards stable and efficient training of verifiably robust neural networks," in *International Conference on Learning Representations*, 2020.
- [35] M. Balunovic and M. Vechev, "Adversarial training and provable defenses: Bridging the gap," in *International Conference on Learning Representations*, 2020.
- [36] M. E. Akintunde, A. Kevorchian, A. Lomuscio, and E. Pirovano, "Verification of rnn-based neural agent-environment systems," in *Proceedings of the AAAI Conference on Artificial Intelligence*, 2019.
- [37] M. Wu and M. Kwiatkowska, "Robustness guarantees for deep neural networks on videos," *arXiv preprint arXiv:1907.00098*, 2019.
- [38] M. Esmailpour, P. Cardinal, and A. L. Koerich, "A robust approach for securing audio classification against adversarial attacks," *arXiv preprint arXiv:1904.10990*, 2019.
- [39] K. Dvijotham, S. Gowal, R. Stanforth, R. Arandjelovic, B. O'Donoghue, J. Uesato, and P. Kohli, "Training verified learners with learned verifiers," *arXiv preprint arXiv:1805.10265*, 2018.
- [40] Z. Lyu, C.-Y. Ko, Z. Kong, N. Wong, D. Lin, and L. Daniel, "Fastened crown: Tightened neural network robustness certificates," *arXiv preprint arXiv:1912.00574*, 2019.
- [41] Z. Shi, H. Zhang, C.-J. Hsieh, K.-W. Chang, and M. Huang, "Robustness verification for transformers," in *International Conference on Learning Representations*, 2020.
- [42] Y. Jacoby, C. Barrett, and G. Katz, "Verifying recurrent neural networks using invariant inference," *arXiv preprint arXiv:2004.02462*, 2020.
- [43] K. D. Dvijotham, J. Hayes, B. Balle, Z. Kolter, C. Qin, A. Gyorgy, K. Xiao, S. Gowal, and P. Kohli, "A framework for robustness certification of smoothed classifiers using f-divergences," in *International Conference on Learning Representations*, 2019.
- [44] M. Fischer, M. Baader, and M. Vechev, "Certification of semantic perturbations via randomized smoothing," *arXiv preprint arXiv:2002.12463*, 2020.
- [45] P. Warden, "Speech commands: A dataset for limited-vocabulary speech recognition," *arXiv preprint arXiv:1804.03209*, 2018.
- [46] S. Hochreiter and J. Schmidhuber, "Long short-term memory," *Neural Comput.*, vol. 9, no. 8, pp. 1735–1780, Nov. 1997. [Online]. Available: <http://dx.doi.org/10.1162/neco.1997.9.8.1735>
- [47] S. Pascual, A. Bonafonte, and J. Serra, "Segan: Speech enhancement generative adversarial network," *arXiv preprint arXiv:1703.09452*, 2017.
- [48] T. N. Sainath, R. J. Weiss, A. Senior, K. W. Wilson, and O. Vinyals, "Learning the speech front-end with raw waveform cldnns," in *Sixteenth Annual Conference of the International Speech Communication Association*, 2015.
- [49] M. Sahidullah and G. Saha, "Design, analysis and experimental evaluation of block based transformation in mfcc computation for speaker recognition," *Speech Communication*, vol. 54, no. 4, pp. 543–565, 2012.
- [50] R. Jia, A. Raghunathan, K. Göksel, and P. Liang, "Certified robustness to adversarial word substitutions," in *Proc. Empirical Methods in Natural Language Processing (EMNLP)*, K. Inui, J. Jiang, V. Ng, and X. Wan, Eds., 2019, pp. 4127–4140.
- [51] P. Yeh Chiang\*, R. Ni\*, A. Abdelkader, C. Zhu, C. Studor, and T. Goldstein, "Certified defenses for adversarial patches," in *Proc. International Conference on Learning Representations (ICLR)*, 2020.
- [52] G. Singh, T. Gehr, M. Püschel, and M. Vechev, "An abstract domain for certifying neural networks," *Proceedings of the ACM on Programming Languages*, vol. 3, no. POPL, p. 41, 2019.
- [53] M. Balunovic, M. Baader, G. Singh, T. Gehr, and M. Vechev, "Certifying geometric robustness of neural networks," in *Advances in Neural Information Processing Systems*, 2019.
- [54] S. Sabour, N. Frosst, and G. E. Hinton, "Dynamic routing between capsules," in *Proc. Neural Information Processing Systems (NIPS)*, 2017, pp. 3856–3866.
- [55] N. Carlini and D. A. Wagner, "Towards evaluating the robustness of neural networks," in *Proc. IEEE Symposium on Security and Privacy (SP)*, 2017, pp. 39–57.
- [56] A. Paszke, S. Gross, S. Chintala, G. Chanan, E. Yang, Z. DeVito, Z. Lin, A. Desmaison, L. Antiga, and A. Lerer, "Automatic differentiation in pytorch," 2017.
- [57] D. P. Kingma and J. Ba, "Adam: A method for stochastic optimization," *arXiv preprint arXiv:1412.6980*, 2014.
- [58] Y. LeCun, C. Cortes, and C. Burges, "Mnist handwritten digit database," *AT&T Labs [Online]*. Available: <http://yann.lecun.com/exdb/mnist>, 2010.
- [59] Z. Jackson, "Free spoken digit dataset," <https://github.com/Jakobovski/free-spoken-digit-dataset>, 2020.